A 0-D impurity transport model for discharge preparation and real-time application

A. Kallenbach[1], M. Bernert[1], P. David[1], R. Dux[1], ASDEX Upgrade team[2]

[1]*Max Planck Institute for Plasma Physics, D-85748 Garching, Germany,*

[2] *see author list of H. Zohm et al. Nucl. Fusion 2024*

Introduction

A simple transport model was recently developed which allows the prediction of the divertor and core impurity densities based on gas valve fluxes and other engineering parameters [1]. The impurity densities can be used for the prediction of radiative losses, applicable for simple discharge planning or in a flight simulator. The prevailing experimental conditions for this study are high radiative losses, dominated by the seed impurities, close to divertor detachment.

Prediction of impurity densities

For stationary conditions, the neutral concentrations of recycling impurities in the divertor can be related to the their respective gas puff rates, facilitating particle balance and known pumping speeds:

$$c_{z0,div} = \Phi_{z0}/(z\,\Phi_D)\ \times f_s \tag{1}$$

f_s is the ratio of effective pumping speeds between D_2 and the impurities, with typical values between 1.2 ... 1.5 for Ne .. Kr [1]. Core impurity densities are subsequently calculated employing an analytic relation between divertor neutral pressure and midplane separatrix density and an effective inward drift, which has been obtain from a fit to experimental data [1]:

$$n_{z,main} = \tau_z v_{z,in}^{eff} A_{sep} c_{z0,div} n_{e,sep}/V_{main} \tag{2}$$

A_{sep} is the plasma surface area at the separatrix and V_{main} the main plasma volume. The core particle confinement time τ_z is assumed to pe proportional to the plasma current and is set to 0.075 s for I_p= 1 MA. The separatrix electron density is derived from a simple scaling relating it to the neutral divertor pressure, $n_{e,sep} = 2.65 p_0^{0.31}$ [10^{19} m^{-3}, Pa] [2]. The effective inward drift combines the divertor compression and transport from separatrix into the core plasma. It appears to be in first order independent of the plasma conditions.

$$v_{z,in}^{eff} = 0.25\, Z^{0.64} (E_{ion,z}/E_{ion,D})^{6.0}\ \ [m/s] \tag{3}$$

We obtain values of (1.3, 17.3, 3.85, 3 m/s) for (N, Ne, Ar, Kr). Fig. 1 compares the scaling prediction with the measured core impurity densities. Agreement within a factor two is achieved.

Simple analytic model for divertor radiation and power dissipation

The total radiated power produced by post-processing of experimental data is decomposed into elements which can be described by simple models and using real time diagnostics only.

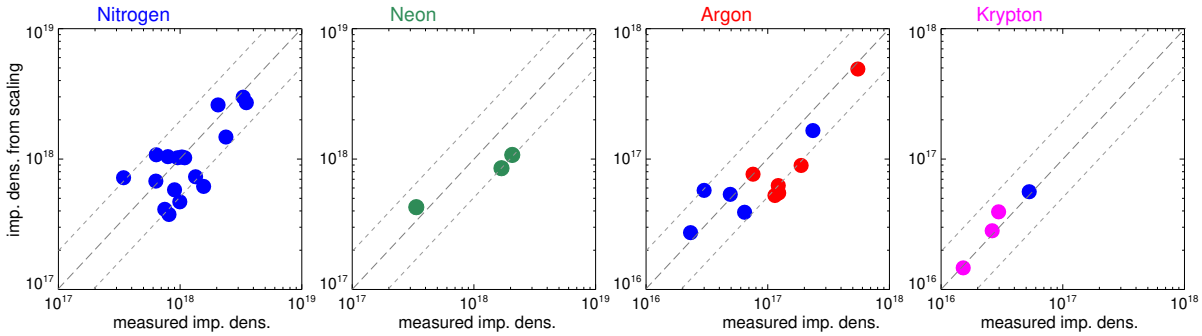

Figure 1: *Impurity densities in m^{-3} predicted by the scaling using engineering parameters only versus measured values (CXRS in case of N, Ne, Ar and SXR+VUV in case of Kr). Overall agreeement is within a factor 2. Impurity densities measured in the presence of strong nitrogen seeding are shown in blue symbols.*

Validation is possible by comparison to direct experimental measurements of impurity densities, radiation and global Z_{eff} which are usually processed post-pulse. For this contribution the data base presented in [1] has been extended by further shots with absolute impurity density measurements, see figure 1. Figure 2 shows the geometrical arrangement used to derive the lower outer divertor radiation as well as the radiation around the X-point from bolometry.

Outer divertor radiation

The power crossing the separatrix at the onset of divertor detachment in the flux tube containing the first power e-folding length can be described as [3]

$$P_{sep}/R|_{det.point} = \frac{1}{1.3} p_0 (1 + \sum_z f_z c_{z,ion}) \cdot (\lambda_{int}/0.005m) \;\; [MW/m,\, Pa,\, m] \qquad (4)$$

About 2/3 of this power is directed towards the outer SOL, and a small fraction of this power will be deposited at the outer limiters [4]. Accordingly, we interprete the term $\frac{1}{2} R \frac{1}{1.3} p_0 \, f_z c_{z,ion} \cdot (\lambda_{int}/0.005m)$ as the radiative loss in the outer SOL caused by the seed impurity Z. λ_{int} is the (broadened) power width close to the target and assumed to scale $\lambda_{int} = 0.005\, m/I_p \; [MA]$. We assume that the divertor impurity radiation, caused mainly by ionized impurity species, is closer related to the impurity flux rather than the impurity density. Therefore, we relate the ion density to the neutral impurity flux, $c_{z,ion} = c_{z0}(m_{D2}/m_z)^{0.5}$. This leads also to better agreement with spectroscopically measured impurity ion densities [5, 1]. The specific radiation weights f_z have been derived by 1D modelling [3], we use the values (18, 45, 90, 180) for (N, Ne, Ar, Kr).

The remaining p_0 term represents dissipation by deuterium, which combines radiation, ionisation, charge exchange and recombination. Figure 3a compares the simple prediction of the divertor impurity radiative losses, using divertor impurity concentrations derived from gas puff with the power measured by bolometry in the lower part of the divertor, see figure 2. As expected, the prediction remains below the measured radiation for low seeding levels, where intrinsic radiators as B or C contribute, and approaches the measurement for high levels of nitrogen seeding.

In accordance with the experiment, only nitrogen allows high radiation in the lower outer divertor. The contribution of deuterium to the measured radiation is expected to be small. As shown in figure 3b, the relative radiation in the upper divertor part and X-point region increases with decreasing T_{div} / increasing degree of detachment. This ratio is overall much higher for Ne compared to N, Ar, Kr. This is assumed to be the result of the much lower divertor compression of Ne, caused by its larger ionization length. At low values $T_{div} \leq 3$ eV, radiation by an X-point radiator contributes to the upper bolometer chord-set. Figure 3c compares the dissipated power according to eq 4 with $P_{sep} = P_{heat} - P_{rad,main}$. Again, half of P_{sep} is used to take into accout the power flux fraction directed into the outer divertor.

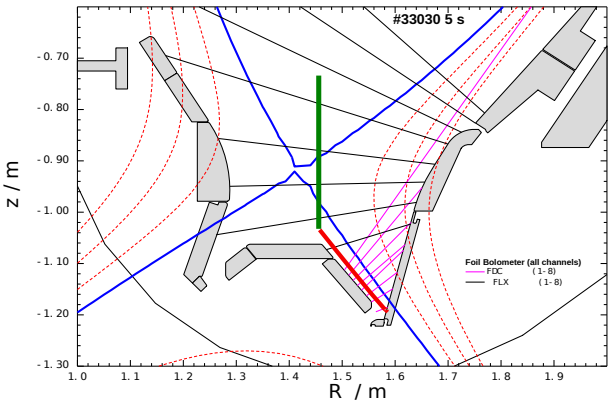

Figure 2: *Bolometer setup for the simple and fast determination of the radiation in the outer divertor and region around X-point. The line-integrated power densities measured by the shown bolometer chords are multiplied by the surface areas indicated by the two bars projected into the poloidal plane (surface area* $l_{bar} \times 2\pi\overline{R}_{bar}$*).*

The dissipation includes the hydrogenic loss terms, which are partly not recorded by bolometry (CX, ionisation). For the experimental conditions considered here, with the outer divertor in the vicinity of detachment, the inner divertor is always detached in ASDEX Upgrade. We expect

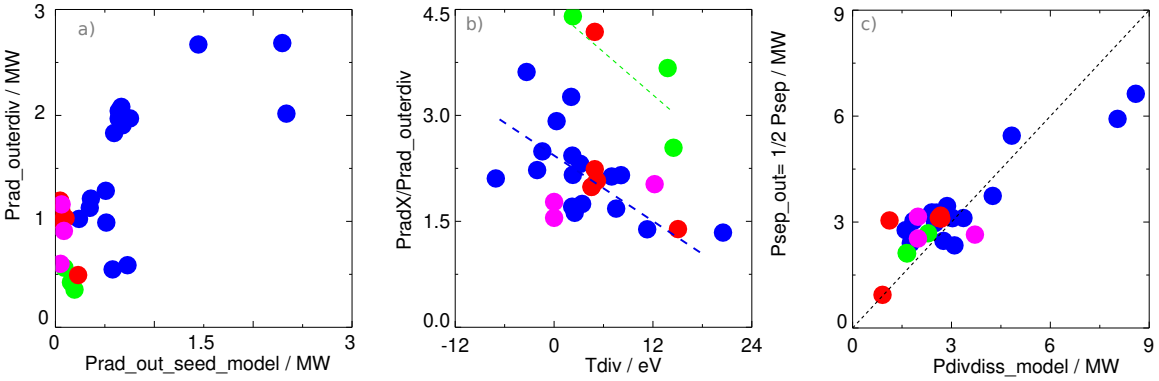

Figure 3: *a) Comparison of the radiation in the lower outer divertor (red bar in fig. 2) with the simple model. b) Ratio of radiation around the X-point and lower divertor radiation vs. divertor temperature* T_{div}*. Lines only to guide the eye. c) Predicted dissipated power in the outer divertor at detachment onset versus approximate experimental power into the outer divertor, 1/2* P_{sep}*.*

full dissipation of the one third of P_{sep}, flowing towards the inner target, by radiation and effects of neutrals for the present conditions around partial detachment of the outer divertor. Very high divertor dissipation is only obtained with N for AUG conditions, which is the result of the varying divertor compression of the different impurities and the limiting core radiative losses.

Main plasma radiation

The impurity core concentrations predicted by the model can be used to predict main chamber radiation losses via $\Sigma_z\ L_z\ c_z\ n_e^2$. Here, non-Corona effects entering L_z, e.g. by charge exchange with neutral deuterium, are important for the radiation of seed impurities in the outer core region. Despite the plasma Z_{eff} from bremsstrahlung is generally well reproduced by the indvidual impurities, the total core radiation is often under-predicted. Possible reasons are an underestimation of non-Coronal effects, e.g. by charge exchange with neutral D, or the contribution of SOL radiation from the high field side, which is not accounted for by the core radiation model. Recently, the model described has been integrated into the flight simulator Fenix [6] to provide the outer core impurity density as boundary condition.

Discussion and conclusions

A simple analytial model was set up for the prediction of impurity densities and radiative losses based on engineering parameters only. The model provides an overview over the radiative operational space of ASDEX Upgrade. It applies to core and divertor radiation for conditions without a strong X-point radiator, for which no simple model yet exists. Substantial radiation levels in the lower outer divertor can be achieved in ASDEX Upgrade only with nitrogen seeding. Neon is not well enough compressed in the divertor due to its long ionisation mean free path, resulting in its radiation to occur as radiative mantle and in the X-point region. Argon and krypton are well compressed in the divertor due to their shorter ionisation mean free paths. However, their high values of the radiative loss function at high temperatures [7] lead to preferential radiation losses in core, pedestal and X-point regions (Ar). SOLPS-ITER modelling suggests that the effect of ionisation mean free path length diminishes with increasing machine size [8]. However, a strict reproduction of the AUG results with modelling is required before the different behaviour can be safely assigned to a divertor size effect.

Acknowledgements

This work has been carried out within the framework of the EUROfusion Consortium, funded by the European Union via the Euratom Research and Training Programme (Grant Agreement No 101052200 - EUROfusion). Views and opinions expressed are however those of the author(s) only and do not necessarily reflect those of the European Union or the European Commission. Neither the European Union nor the European Commission can be held responsible for them.

References

[1] KALLENBACH, A. et al., Nuclear Fusion **64** (2024) 056003.
[2] KALLENBACH, A. et al., Plasma Physics and Controlled Fusion **60** (2018) 045006.
[3] KALLENBACH, A. et al., Plasma Physics and Controlled Fusion **58** (2016) 045013.
[4] REDL, A. et al., Nuclear Materials and Energy **34** (2023) 101319.
[5] HENDERSON, S. S. et al., Nucl. Fusion **58** (2018) 016047.
[6] FABLE, E. et al., Plasma Physics and Controlled Fusion (2021).
[7] PÜTTERICH, T. et al., Nucl. Fusion **59** (2019) 056013.
[8] ROZHANSKY, V. et al., Nuclear Fusion **61** (2021) 126073.